Two-Dimensional Infrared Investigation of *N*-Acetyl Tryptophan Methyl Amide in Solution

Sayan Bagchi, Yung Sam Kim, Adam K. Charnley, Amos B. Smith, III, and Robin M. Hochstrasser*

Department of Chemistry, University of Pennsylvania, Philadelphia, Pennsylvania 19104-6323

Received: November 7, 2006; In Final Form: December 18, 2006

The linear infrared and two-dimensional infrared (2D IR) spectra in the amide-I region of *N*-acetyl tryptophan methyl amide (NATMA) in solvents of varying polarity are reported. The two amide-I transitions have been assigned unambiguously by using ^{13}C isotopic substitution of the carbonyl group. The amide unit at the amino end shows a lower transition frequency in CH_2Cl_2 and methanol, while the acetyl end has a lower transition frequency in D_2O. Multiple conformers exist in CH_2Cl_2 and methanol, but only one conformer is evident in D_2O. The 2D IR cross peaks from the intermode coupling yield off-diagonal anharmonicities 2.5 ± 0.5, 3.25 ± 0.5, and 3.0 ± 0.5 cm^{-1} in CH_2Cl_2, methanol, and D_2O, respectively, which by simple matrix diagonalization yield the coupling constants 8.0 ± 0.5, 8.0 ± 1.0, and 5.5 ± 1.0 cm^{-1}. The major conformer in CH_2Cl_2 corresponds to a C_7 structure, in agreement with that found in the gas phase [Dian, B. C.; Longarte, A.; Mercier, S.; Evans, D. A.; Wales, D. J.; Zwier, T. S. *J. Chem. Phys.* **2002**, *117*, 10688−10702] with intramolecular hydrogen bonding between the acetyl end C═O and the amino end N−H. The backbone dihedral angles (φ, ψ) are determined to be in the ranges of (−55 ± 5°, 30 ± 5°), (120 ± 10°, −20 ± 10°), and (±160 ± 10°, ±75 ± 10°) in CH_2Cl_2, methanol, and D_2O, respectively.

1. Introduction

Protein structure prediction requires development of incisive tools to probe and characterize different peptide conformations in the condensed phase. Systematic investigations on vibrational spectroscopy have shown that the amide-based infrared transitions of the polypeptide backbone are sensitive to the structure of the proteins.[1,2] This structural sensitivity mainly arises from the vibrational couplings between the amide-I oscillators and intramolecular hydrogen bonding, both of which depend on the relative position, orientation, and connectivity of the peptide units. Other factors such as configurational disorder, intra- or intermolecular hydrogen bonding, and fast vibrational relaxation broaden the linear infrared absorption spectra resulting in relatively featureless bands, making it difficult to analyze and interpret the underlying molecular structure.

Multidimensional coherent spectroscopic techniques were commonly used in multiple-pulse NMR to disentangle the complex featureless spectra of many interacting spins by spreading them along multiple axes.[3] The two-dimensional infrared spectroscopy (2D IR) technique[4−8] spreads the vibrational response into two dimensions and allows for the separation of overlapping infrared features; also the structure sensitive vibrational anharmonicities of specific bands, the mechanical coupling between molecular vibrations, and the line-shape parameters can be obtained, making this technique more sensitive to the molecular structure than linear IR. The 2D IR method provides a direct approach to measure the coupling and specific angular relations between the amide units, thereby providing more model-free information about the peptide structure compared with linear IR experiments. In addition, by separating the molecular structural distributions or inhomogeneous broadening from homogeneous relaxation processes, 2D IR spectra are line-narrowed compared with FTIR spectra.

Experimental and theoretical 2D IR studies have been performed to characterize the conformationally dependent frequencies of the amide-I band profiles (primarily C═O stretches) of several small peptides in the condensed-phase, exploiting their large IR cross-sections and freedom from spectral overlap with other modes. The coupling of these modes is vital to vibrational spectroscopic analysis of the secondary structure. The first investigations of the couplings involved detection of individual cross peaks and relating their intensities and anisotropies to known structures such as a cyclic pentapeptide[9] but were soon extended to the determination of the previously undetermined P_{II} structure of trialanaine[10] by exploring the excitonic states of amide-I vibrations. Studies of solvent-dependent conformations of acetylproline amine[11] from the polarization dependence of the cross-peak intensities by Zanni et al. exposed multiple conformations in $CDCl_3$, but only one dominant conformer in D_2O. Theoretical simulations of linear infrared, vibrational circular dichroism (VCD), and 2D vibrational spectra of acetylproline were performed,[12,13] and the line shapes of the simulated 2D IR photon echo spectra were found to be quantitatively similar to the above-mentioned experimental results.[11] Recent investigations by 2D IR on the alanine dipeptide gave results consistent with a P_{II} conformation.[14] The two-dimensional infrared technique was applied to larger polypeptides, and the measurements of the magnitudes and signs of the coupling between the amide modes in an α-helical conformation were determined from double isotope labeling experiments.[15−17] Multiple isotope editing combined with VCD has been used by Keiderling and co-workers[18] to elucidate selective coupling of amide-I modes labeled at different positions of the peptide backbone of the α-helical peptide.[16] Combining several theoretical methods,[19−23] a systematic computational methodology has been developed by Cho and co-workers for the

* Corresponding author. Telephone: 215-898-8203. Fax: 215-898-0590. E-mail: hochstra@sas.upenn.edu.

10.1021/jp067348m CCC: $37.00
Published on Web 02/28/2007

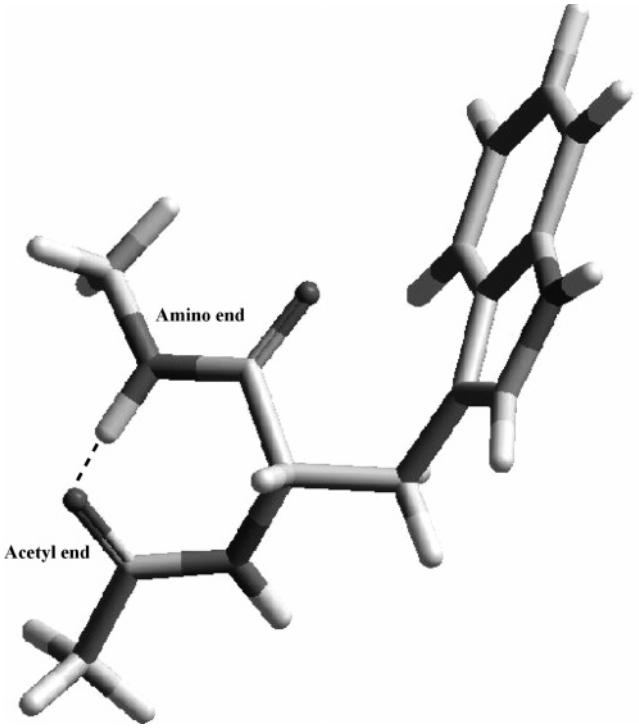

Figure 1. C_7 structure of NATMA The dashed line defines the intramolecular hydrogen bonding between the acetyl end carbonyl (ball and stick) and the amino end N−H. (The tryptophan ring orientation is adopted from ref 54.)

numerical simulation of 2D IR spectra of polypeptides in solutions. Using this approach, 2D IR spectra of isotope-labeled aqueous α-helical polyalanine solutions[24] were numerically simulated and compared favorably with the earlier experimental results.[16,18] Simulations of IR and VCD spectra of helical peptides[25] have characterized the solvent effects of oligopeptide vibrational spectra. Other secondary structural motifs such as parallel and antiparallel *β*-sheets were also investigated using the 2D IR method. Two-dimensional IR signatures of the correlation spectrum of antiparallel *β*-sheets were reported from experiments on polylysine.[26] This study was supported by theoretical calculations which reveal spectroscopic markers that claim to distinguish parallel from antiparallel *β*-sheets, and hairpins from extended sheets.[27] A series of AM1 and ab initio calculations on the local amide-I mode frequencies and coupling constants in multiple-stranded parallel[28] and antiparallel[29,30] *β*-sheets were also reported. Local structures of *β*-hairpin isotopomers (tryptophan zippers) were investigated by 2D IR and ab initio theory,[31−33] and theoretical calculations on a polyalanine-based *β*-hairpin[34] showed that the effect of solvent on the amide-I vibrations is dependent on the local conformation. Recent work on octapeptide 3_{10} helices and α-helices have revealed the different two-dimensional spectral signatures of these structures,[35] suggesting avenues for elucidating the role of these motifs in protein folding events. Other nonlinear methods like polarized Raman spectroscopy, combined with FTIR and electronic circular dichroism (ECD) spectroscopy are also used for the investigation of peptide structures. Schweitzer-Stenner et. al. have studied the conformational sensitivity of the amide-III vibrational mode in a series of dipeptides[36,37] and tripeptides[38,39] in water. Similar experiments done on an octapeptide $(AAKA)_2$ show existence of a mixture of PPII and *β*-strand conformtations in aqueous solution.[40] Electrostatic density functional theory (DFT) mapping[41,42] has been a recent development in the theoretical predictions of the fundamental

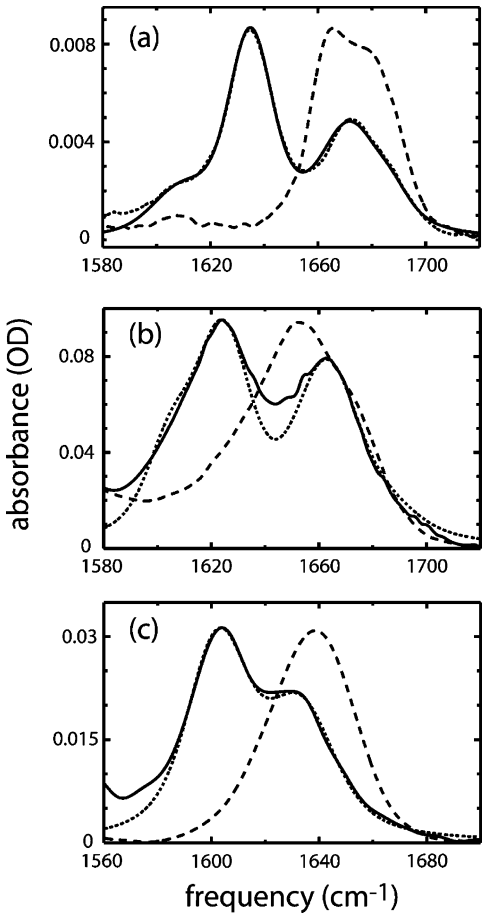

Figure 2. Linear FTIR spectra of the unlabeled NATMA(dashed), $C^{13}{=}O^{16}$-labeled NATMA at the amino end (solid) and the Fourier transform of the linear response function (dotted) for the labeled NATMA in (a) methylene chloride, (b) methanol, and (c) D_2O.

and combination bands of several amide modes, since including a solvent effect and realistic structure fluctuations is expected to bring a substantial increase in the accuracy of the simulation of the nonlinear response. The maps include geometry fluctuations in response to the solvent-induced electrostatic potential, making a more direct comparison with the condensed-phase nonlinear experimental spectra than do gas-phase ab initio maps. This methodology was used to simulate the vibrational spectra of *N*-methylacetamide (NMA)[43] and a pentapeptide (Ala−Ala-Aib-D-Ala-Ala-$NHCH_3$).[43] Such calculations on NMA[43] brought the vacuum frequency of the amide-I mode much closer to the observed value.[19,44]

Experimental techniques such as UV and IR/UV double resonance laser spectroscopy have been used to investigate peptide structure and conformation in the gas phase, providing possibilities for direct comparison of the results with vacuum computations.[45−50] Pioneering work by Levy and co-workers on the spectra of tryptophan[45] was followed by the efforts of several other experimental groups on other amino acids and peptides. Gas phase studies have been used to investigate amino acids such as phenylalanine,[47] tryptophan,[48] and homo-[46] and hetero-dipeptides.[49,50] In a detailed experimental study of isolated *N*-acetyl tryptophan methyl amide (NATMA) molecules, Zwier et al.[51−53] reported the existence of many energetically accessible conformational minima.

The present 2D IR work is aimed at investigating the solution phase structural features of NATMA (see Figure 1) to compare the results in solvents of different polarity with those found in the gas phase.[51−53] NATMA being a relatively small dipeptide,

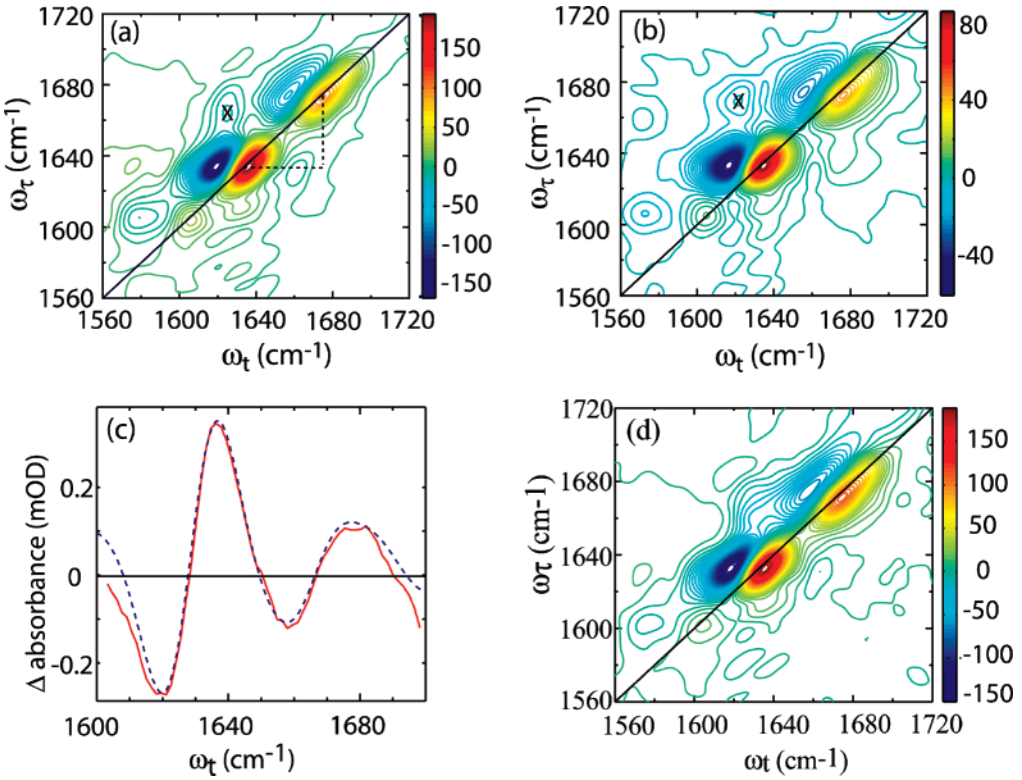

Figure 3. Real part of absorptive 2D IR spectra of isotopically substituted NATMA in methylene chloride for ⟨zzzz⟩ polarization at (a) $T = 0$ and (b) $T = 1$ ps. (c) Comparison of pump−probe spectrum and the projection of the absorptive 2D IR spectrum for ⟨zzzz⟩ onto the ω_t axis at $T = 0$. (d) Real part of absorptive 2D IR spectra of isotopically substituted NATMA in methylene chloride for ⟨zxxz⟩ polarization at $T = 0$.

with its amide-I modes at very similar frequencies, required isotopic labeling to separate the otherwise spectrally overlapping modes. The amide-I carbonyl of the *N*-methylamino end was substituted with $^{13}C{=}^{16}O$, thus lowering its transition frequency by ca. 40 cm^{-1}. This shift allows spectra of the *N*-methylamino and acetyl ends of the peptide to be discriminated. The coupling between the amide-I modes, the frequency positions, structural conformations, and other signatures in 2D IR spectra showed significant differences in the structure of NATMA in the gas phase, nonpolar solvents, and aqueous solutions.

2. Experimental Section

Sample Preparation. *N*-Acetyl tryptophan methyl amide (NATMA) was prepared according to published protocols.[52,54] Its ethyl ester (Aldrich) was dissolved in methanol and treated with 20 equiv of methylamine (2.0 M in methanol) for 48 h. Recrystallization from 1:1 ethanol/hexanes provided NATMA as a white crystalline solid. *N*-acetyl-1-[^{13}C]-tryptophan methyl amide (^{13}C-NATMA) was prepared in two steps from 1-[^{13}C]-L-tryptophan (Cambridge Isotope Laboratories). In step 1, acetyl chloride (3.0 equiv) was dissolved in CH_2Cl_2 and treated with HOBt (3.2 equiv) and diisopyropylethyl amine (2.0 equiv) for 20 min to generate the acyl-HOBt adduct. This reagent was then added to a solution of 1-[^{13}C]-L-tryptophan (1.0 equiv) and diisopropylethyl amine (2.0 equiv) in CH_2Cl_2 at 0 °C. After 24 h at room temperature, the reaction was quenched with 10% aqueous $NaHSO_4$, filtered, and extracted with ethyl acetate. The combined organic layers were dried with $MgSO_4$ and concentrated in vacuo.

The crude product from step 1 was dissolved in DMF and treated with 1-ethyl-3-(3′-dimethylaminopropyl)-carbodiimide·HCl (EDC, 1.3 equiv) and diisopropylethyl amine (3.0 equiv) at 0 °C. After 1 h, methylamine (10 equiv, 2.0 M in THF) was added, and the reaction was stirred at room temperature for 24 h. Standard aqueous workup and purification via preparative TLC (10% methanol/CH_2Cl_2) and finally recrystallization (1:1 ethanol/hexanes) provided ^{13}C-NATMA. NATMA and ^{13}C-NATMA were characterized by NMR, IR, and high-resolution mass spectrometry.

Both the unlabeled NATMA and that labeled by $^{13}C{=}^{16}O$ at the amino end were dissolved in methylene chloride, methanol, and D_2O separately; the optical densities of the *N*-methylamino end amide-I peaks were 0.01, 0.1, and 0.03, respectively, using CaF_2 cells and a 56 μm path length. NATMA is much more soluble in methanol than either of the other solvents.

Linear IR Spectroscopy. The Fourier transform infrared (FTIR) absorption spectra were recorded on a Perkin-Elmer 2000 Explorer spectrometer with 1.0 cm^{-1} resolution at room temperature.

Two-Dimensional IR Spectroscopy. The multidimensional IR spectra were obtained using heterodyned spectral interferometry with the laser arrangement described previously.[4,16,55] Three Fourier transform limited 75 fs pulses (wave-vectors k_1, k_2, and k_3) with energy of ca. 400 nJ each were incident on the sample. The signal in the phase matching direction $-k_1 + k_2 + k_3$ was detected by heterodyning it with a local oscillator (LO) pulse, which preceded the signal pulse by ∼1500 fs. The time interval between the first and the second pulses is denoted by τ, between the second and the third pulses by T, and that of the third pulse and the detected signal by t. The sequence where k_1 arrives earlier than k_2 gives rise to the rephasing (R) signal; the non-rephasing (NR) signal is from the pulse sequence where k_2 arrives before k_1. The signal and the LO were combined at the focus of the monochromator (with a groove density 50 lines/mm), and the heterodyned signal created was detected by a 64-element HgCdTe array detector. Each detector element is 200 μm in width and 1 mm in height. The experimental raw data

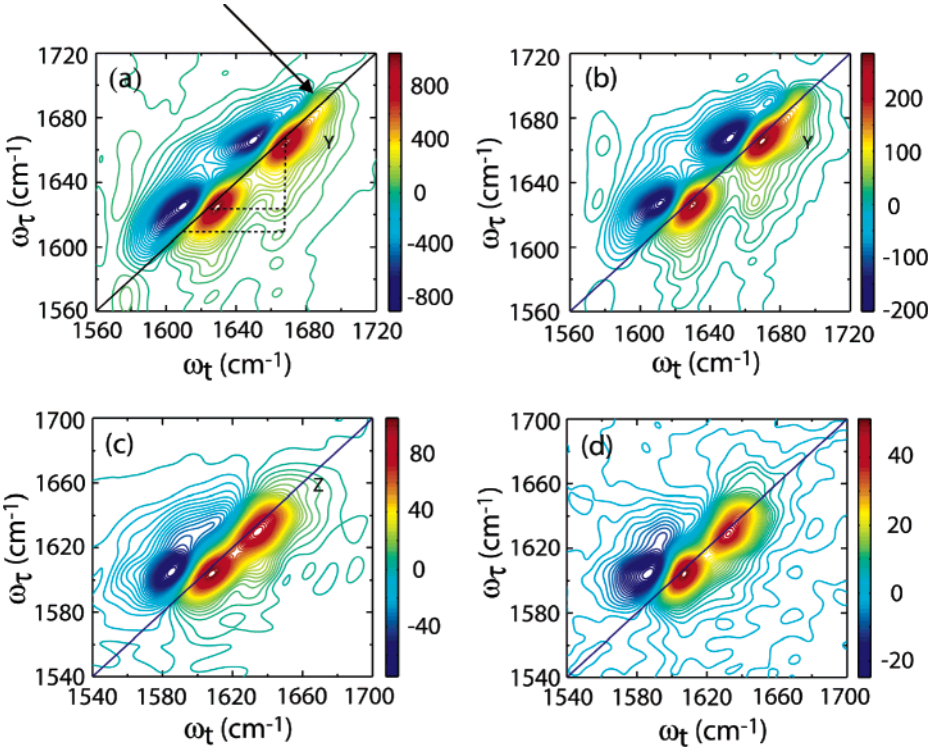

Figure 4. Real part of absorptive 2D IR spectra of isotopically substituted NATMA in methanol at (a) $T = 0$, (b) $T = 1$ ps and in D_2O at (c) $T = 0$, (d) $T = 500$ fs.

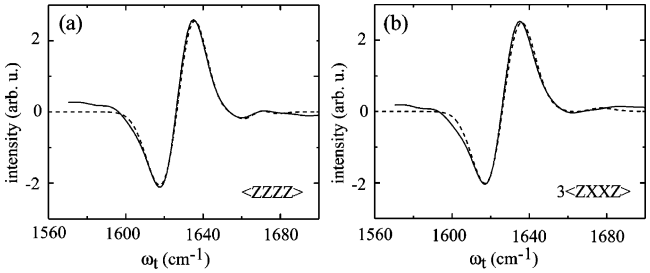

Figure 5. Trace along $\omega_\tau = 1635$ cm^{-1} of the real parts of the 2D IR spectra for NATMA in methylene chloride as described in the text and its fits for (a) ⟨*zzzz*⟩ polarization condition and (b) ⟨*zxxz*⟩ polarization condition.

collected in this procedure were in the form of a two-dimensional array $S(\tau,\lambda;T)$ of time (in 2 fs steps) and wavelength (in ~15 nm steps). By performing an inverse Fourier transform to the time domain followed by a Fourier transform to the frequency domain, this raw data $S(\tau,\lambda;T)$ was converted to $\bar{S}(\tau,\omega_t;T)$. The spectra obtained as combined frequency time data sets are defined as $\bar{S}_R(\tau,\omega_t;T)$ and $\bar{S}_{NR}(\tau,\omega_t;T)$. The detailed protocols of data processing have been described previously.[14] The pulse center frequency was chosen in the region between the two amide-I transition frequencies; for solutions of NATMA in methylene chloride, methanol, and D_2O, the center frequency was 1645, 1635, and 1620 cm^{-1}, respectively. The slope of the zero contour line separating the $v = 0 \rightarrow v = 1$ and $v = 1 \rightarrow v = 2$ regions was employed as a useful measure of the 2D IR shape changes with waiting time (T), caused by spectral diffusion, including dynamical exchange processes.[56,57]

3. Experimental Results

FTIR Spectrum of NATMA. The linear IR spectra for unsubstituted and ^{13}C isotopically labeled NATMA (at the amino end) in CH_2Cl_2, methanol, and D_2O are shown in Figure 2. The spectrum of the unlabeled compound in CH_2Cl_2 showed one broad asymmetric amide-I band, clearly composed of more than one peak. When the amino end $^{12}C{=}^{16}O$ was replaced by $^{13}C{=}^{16}O$, two separated amide-I bands were observed, the isotopically substituted amide-I band being red-shifted by ca. 30 cm^{-1}. The peak positions and the intensities were obtained by curve-fitting the spectra with Voigt profiles.[14] The lower frequency band (*N*-methylamino end) in CH_2Cl_2 showed a transition at 1634 cm^{-1}, while the higher frequency band (acetyl end) peaked at 1672 cm^{-1}. An additional transition at the acetyl end was observed as a shoulder at 1687 cm^{-1} with an intensity of 25% of the band at 1672 cm^{-1}. The linear IR spectrum at the N−H stretch region in CH_2Cl_2 (data not shown) was not analyzed in detail, but it was composed of multiple peaks, some of which corresponded to free N−H and other red-shifted broader regions corresponding to hydrogen-bonded N−H.

In methanol, the unlabeled dipeptide also exhibited a broad asymmetric amide-I band, composed of multiple peaks (Figure 2b). After isotopic substitution, two main bands were observed. When curve-fitted to Voigt profiles, the lower frequency *N*-methylamino end band consisted of two peaks, one at 1625 cm^{-1} and another having 25% the absorption strength, at 1605 cm^{-1}. The higher frequency acetyl end also consisted of two overlapping Voigt profiles, a band at 1664 cm^{-1} which was four times stronger than the one at 1688 cm^{-1}.

In D_2O (Figure 2c), the broad asymmetric band obtained from the FTIR experiment of the unlabeled compound could be curve-fitted using Voigt profiles into two components having different intensities. The acetyl end amide-I mode was red-shifted by 14 cm^{-1} from the stronger *N*-methylamino end transition. This ordering is opposite to the findings in the other two solvents. In this example the modes must be more delocalized than in the other solvents, but the acetyl and *N*-methylamino notations are retained for convenience. Two separate groups of amide-I bands were observed for the isotopically labeled NATMA in D_2O with the *N*-methylamino end transition frequency at 1603 cm^{-1} and that of the acetyl end at 1633 cm^{-1}. The unlabeled

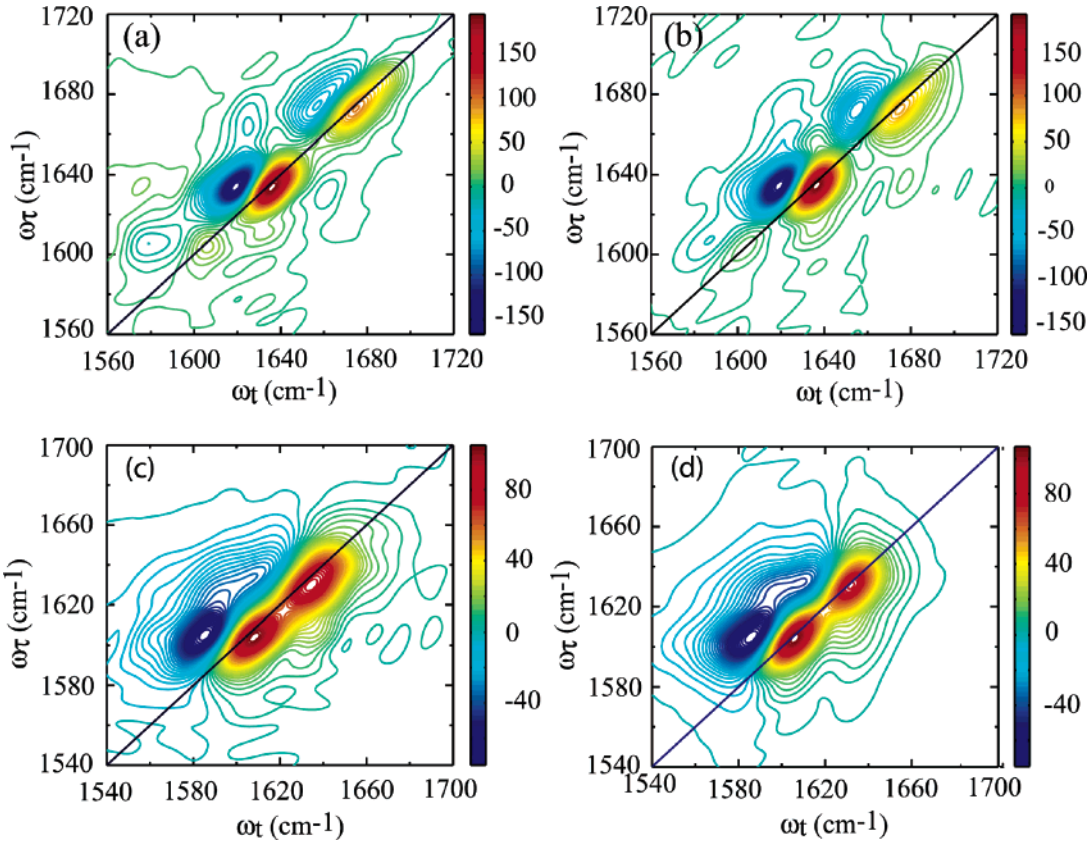

Figure 6. Real part of the experimental absorptive 2D IR spectra of isotopically substituted NATMA in (a) CH_2Cl_2 and (c) D_2O and real part of the simulated absorptive 2D IR spectra of isotopically substituted NATMA in (b) CH_2Cl_2 and (d) D_2O at $T = 0$.

spectrum in Figure 2c shows from its asymmetry that there is a weaker underlying band in the low-frequency region.

Two-Dimensional IR Spectra. The absorptive 2D IR spectra $\underline{S}(\omega_\tau,\omega_t;T)$ shown in Figures 3 and 4 were obtained by combining the rephasing $\bar{S}_R(\tau,\omega_t;T)$ and the non-rephasing spectra $\bar{S}_{NR}(\tau,\omega_t;T)$ along the τ-axis (τ was scanned up to 2 ps for both the R and NR data) and Fourier transforming along the same axis. The combined data used $\bar{S}_{NR}(\tau,\omega_t;T)$ values for negative τ and $\bar{S}_R(\tau,\omega_t;T)$ values for positive τ. The data obtained from pump−probe experiments were used for adjusting the phase of combined 2D IR spectra by comparing projections onto the ω_t axis to the pump−probe data (Figure 3c). The individual rephasing and non-rephasing spectra also provided useful information regarding the existence of underlying peaks. The absorptive 2D IR spectra of a single oscillator consist of ellipses elongated along the diagonal ($\omega_t = \omega_\tau$) direction. At small values of T, before spectral diffusion homogenizes the spectrum, the diagonal length is a measure of the total dephasing, which includes population relaxation, inhomogeneous broadening, and motionally narrowed frequency fluctuations, whereas the antidiagonal width is determined by the homogeneous part of the dephasing rate.

The 2D IR spectrum of isotopically substituted NATMA in CH_2Cl_2 shown in Figure 3 has a number of pairs of diagonal peaks with each consisting of a $v = 0 \rightarrow v = 1$ transition on the diagonal and a $v = 1 \rightarrow v = 2$ transition shifted along the horizontal axis by the diagonal anharmonicity of ca. 15 cm^{-1}. The peak at 1634 cm^{-1} originates from the amide-I stretching mode of the *N*-methylamino (isotopically labeled carbonyl, $^{13}C{=}^{16}O$) and that at 1672 cm^{-1} from the amide-I mode of the acetyl end. The acetyl end peak is significantly more elongated along the diagonal. A clear cross-peak (marked X in Figure 3a,b) is evident, indicating that the two amide-I modes at 1635 and 1672 cm^{-1} in NATMA are coupled. Another pair of weak peaks is evident at around 1605 cm^{-1}. This region is unlikely to be amide-I because its anharmonicity (35 cm^{-1}) is too large. Neither is it caused by aggregation, as evidenced by concomitant study of the tryptophan UV absorption.

In methanol, main diagonal peaks were observed as shown in Figure 4a,b. The peak at 1625 cm^{-1} corresponds to the *N*-methylamino end and the peak at 1664 cm^{-1} to the acetyl end. A low-probability structure is indicated by the weak diagonal peaks appearing at 1688 cm^{-1} (marked with the arrow). There is an obvious cross-peak between the *N*-methylamino and acetyl end peaks. There are at least three structures in methanol, as indicated by the connecting lines in Figure 4a. In D_2O, both transitions were red-shifted compared with the other solvents with the amino end transition appearing at 1603 cm^{-1} (Figure 4c,d) and the acetyl end transition at 1634 cm^{-1}. A cross-peak could be seen between these transitions. The anharmonically shifted peak of the acetyl end carbonyl is interfering with the cross-peak, which causes the signal amplitude to be diminished in the $v = 1 \rightarrow v = 2$ region.

Waiting Time Dependence. The waiting time (T) dependences of the 2D IR spectra of NATMA in CH_2Cl_2, MeOH, and D_2O have been measured and illustrated at a few values of T in Figures 3b and 4b,d, respectively. One effect of increasing the waiting time is the decrease in intensity of the 2D IR spectra. In the case of NATMA in methanol, the population relaxation of the $v = 1$ states of the two acetyl end peaks at 1664 and 1688 cm^{-1} are 800 fs and 1 ps, respectively. The difference in population relaxation rate changes the peak intensity ratio of these bands, and the weak peak at 1688 cm^{-1} becomes more prominent as T increases to 4 ps (data not shown). An intramode

TABLE 1: Parameters Used in the Simulation of the 2D IR Spectra[a]

	solvent = CH_2Cl_2				solvent = MeOH				solvent = D_2O	
param	NMA_1[b]	NMA_2[b]	Ac_1[c]	Ac_2[c]	NMA_1[b]	NMA_2[b]	Ac_1[c]	Ac_2[c]	NMA[b]	Ac[c]
ν (cm^{-1})	1634	1634	1672	1687	1605	1625	1664	1688	1603	1633
σ (cm^{-1})	5.7	5.6	7.1	4.3	6.0	6.8	8.5	7.2	8.1	7.2
Γ (cm^{-1})	3.4	3.4	5.0	2.6	3.0	4.0	4.8	5.5	5.5	6.5
Δ (cm^{-1})	13.5 ± 0.5				17.5 ± 1.0				17.0 ± 1.0	
$\Delta_{1,2}$ (cm^{-1})	2.5 ± 0.5				3.25 ± 0.5				3.0 ± 0.5	
$\lvert\beta\rvert$ (cm^{-1})	8.0 ± 1.0				8.5 ± 1.0				5.5 ± 1.0	
θ	$112 \pm 5°$ (or $(180-112) \pm 5°$)				$100 \pm 5°$ (or $(180-100) \pm 5°$)				$75 \pm 5°$ (or $(180-75) \pm 5°$)	
(φ, ψ)	$(-55 \pm 5°, 30 \pm 5°)$				$(120 \pm 5°, -20 \pm 5°)$				$(\pm 160 \pm 5°, \pm 75 \pm 5°)$	

[a] The error bars in the table correspond to the experimental errors; the mean values of these results are used for the 2D IR simulation. σ and Γ refer to the standard deviation of the Gaussian inhomogeneous distribution and the pure dephasing rate of the 0−1 vibrator, respectively. Δ denotes the diagonal anharmonicity, $\Delta_{1,2}$ the off-diagonal anharmonicity and $|\beta|$ is the coupling magnitude. The parameters (ν, σ, and Γ) shown for methanol were only used to simulate the linear spectrum because of the spectral diffusion mentioned in the text. [b] NMA denotes the amide-I mode at the *N*-methylamino end. [c] Ac denotes the amide-I mode at the acetyl end; the subscripts 1 and 2 designate multiple peaks.

cross-peak (labeled Y in Figure 4a,b) between 1664 and 1688 cm^{-1} became apparent at the larger T values. The 2D IR spectra of NATMA in D_2O show evidence of spectral diffusion with the diagonal peaks standing up more vertically as T is increased from 0 to 500 fs. A detailed analysis of the T dependence of NATMA in D_2O is currently underway and has not been included in this present work.

Polarization Dependence. The spectra of NATMA in methylene chloride, methanol and water have each been obtained in $\langle zzzz \rangle$ and $\langle zxxz \rangle$ polarization conditions, where x, y, and z are orthogonal laboratory axes. The excitation and the local oscillator pulses all have the same laboratory polarization in the case of $\langle zzzz \rangle$; for $\langle zxxz \rangle$ the polarization of the k_2 and k_3 beams have been rotated and are perpendicular to k_1 and k_{LO}. Parts a and d of Figure 3 show the real parts of the absorptive spectra of isotopically labeled NATMA in methylene chloride for the two different polarization conditions.

Parts a and b of Figure 5 show slices from the 2D IR spectra at $\langle zzzz \rangle$ and $\langle zxxz \rangle$ polarization conditions. This figure is obtained from the 2D IR spectra by the procedure:

$$\sum_{\omega_\tau} [\underline{S}_R(-\omega_\tau,\omega_t;0)+\underline{S}_{NR}(\omega_\tau,\omega_t;0)]G(\omega_\tau-\omega_0,\sigma)$$

where the sum is on all the discrete values of ω_τ in the whole spectral region for a given set of polarization conditions; ω_0 was set to 1635 cm^{-1}. The introduction of the Gaussian function $G(\omega_\tau-\omega_0,\sigma)$ with a standard deviation (σ) of 8 cm^{-1} optimized the signal-to-noise ratio of the slice but did not distort its shape along ω_t.

4. Simulation of 2D IR Spectra

The absence of significant dynamics of NATMA in CH_2Cl_2 and D_2O from the waiting time dependent data sets suggests that the simple simulation methods using a Bloch model are reasonable for these solvents. The data in methanol cannot be treated in the same way because it shows obvious variations with waiting time (Figure 4a,b) that we attribute to the hydrogen bond dynamics occurring on the picosecond time scale. The peak positions, the intensities, and the line widths in the linear spectrum were therefore obtained by curve fitting using overlapping Voigt profiles. The widths obtained in this manner were used to compute the inhomogeneous and homogeneous relaxation parameters for the calculation of the response functions[58] in the 2D simulation. The final simulated spectra were least-squares-fitted to the experimental 2D IR spectrum. The diagonal anharmonicity, angles between the oscillators, and the relaxation time factors of the $v = 2$ states were varied during the least-squares fitting of the 2D spectra. Figure 6 shows the simulated 2D IR spectra along with the experimental spectra of NATMA in methylene chloride and water. The diagonal anharmonicities obtained from 2D IR simulation for NATMA in methylene chloride and D_2O are 13.5 and 17 cm^{-1}, respectively. Table 1 contains all the parameters used in the simulation of the 2D IR spectra.

5. Discussion

By means of supersonic expansion experiments, Zwier and co-workers reported the existence of many energetically accessible conformational minima of NATMA. The conformations observed in the gas phase belonged solely to the C_5 and C_7 conformer families. The lowest energy C_5 and C_7 structures were nearly isoenergetic, despite the large difference in the peptide backbone configurations. The C_5 conformers have an extended dipeptide backbone, while that of the C_7 structure (Figure 1) is a seven-membered hydrogen-bonded ring joining the NH of one amide to the carbonyl of the other.

The low-polarity non-hydrogen bonding solvent CH_2Cl_2 was chosen to minimize the solvent effects and to have a reasonably good chance of finding the gas phase structures. In the 2D IR spectrum of isotopically substituted NATMA in CH_2Cl_2 at $T = 0$, the higher frequency peak was strongly elongated along the diagonal. The elongation, as evident from Figure 3, revealed a wide inhomogeneous distribution of frequencies stretching from $\sim$1670−1690 cm^{-1}, corresponding to significant structural disorder at the acetyl end carbonyl consisting of two main peaks at 1672 and 1688 cm^{-1}. The curve fitting of the linear IR spectrum of NATMA in CH_2Cl_2 required incorporation of two peaks near 1634 cm^{-1}, both corresponding to *N*-methylamino end transitions. Therefore there are probably at least two structural conformers of NATMA in CH_2Cl_2, with the most dominant conformer being hydrogen-bonded at the acetyl end but not at the *N*-methylamino end. The 2D IR spectrum of a vibrator with a larger inhomogeneity is elongated more along the diagonal, so the slope of the zero contour line separating the out of phase $v = 0 \rightarrow 1$ and $v = 1 \rightarrow 2$ transition region is reduced. These slopes were measured for all 2D IR spectra.[17] The slope at the *N*-methylamino end transition region was larger than that at the acetyl end region in both methanol and CH_2Cl_2, which is consistent with an internally hydrogen-bonded structure involving the acetyl end carbonyl. Therefore, the main conformer in CH_2Cl_2 has a striking similarity with the C_7 conformer predicted in the gas-phase results in terms of hydrogen bonding. The geometry of this conformer in CH_2Cl_2 is discussed again later in this paper with reference to the cross-peak in polarization dependent experiments and the mode coupling.

Multiple cross peaks in the 2D IR spectrum of NATMA in methanol signifies the existence of multiple structures, the major

one being hydrogen-bonded at the acetyl end and non-hydrogen-bonded at the *N*-methylamino end. There is at least one other minor structure clearly evident from the other cross peaks, as indicated by the connecting lines in Figure 4a. The 2D IR spectra in methanol (Figure 4a,b) showed an enhancement with increased T of the cross-peak in Figure 4a,b, marked with Y between the transitions at 1664 and 1688 cm^{-1}. This cross-peak feature suggests that two transitions differ in their solvent hydrogen bond configurations and that exchange of this configuration is occurring on the picosecond time scale. Such phenomena have been established in other recent examples.[6] The time scale of these changes in shape is ca. a few picoseconds, so it appears to be too fast to be attributed to interchanging peptide structures. It is more likely caused by rapidly interchanging solvent configurations.

In D_2O, both the acetyl end and *N*-methylamino end carbonyls were red-shifted compared with CH_2Cl_2 and methanol. The presence of the cross-peak (above the diagonal line) partially cancels the anharmonically shifted peak from the acetyl end amide-I transition. This was confirmed by the simulation shown in Figure 6. A very weak but definitive transition appeared at 1670 cm^{-1} (marked as Z in Figure 4c). This peak most probably originates from the free acetyl end transition. The population of this conformer is no more than 15% of the major conformer that has hydrogen bonding present at both acetyl and *N*-methylamino ends. The slope of the zero contour line separating the $v = 0 \rightarrow 1$ and $v = 1 \rightarrow 2$ transitions at the *N*-methylamino and acetyl end regions in D_2O were more or less equal (Figure 4c), suggesting similar inhomogeneity (originating from hydrogen bonding to solvent in this case) at the *N*-methylamino and acetyl ends.

Angle between the Dipoles. Previous work[14,55,59] has shown that the angle between the two transition dipoles can be calculated from polarization dependent 2D IR experiments, although dealing with the data requires caution.[12] At two different polarization conditions ($\langle zzzz \rangle$ and $\langle zxxz \rangle$), the $\langle zzzz \rangle$ signal for the diagonal peaks is three times that of $\langle zxxz \rangle$. For the cross peaks, the $\langle zzzz \rangle$ polarization signal (Figure 3a) is proportional to $(4P_2 + 5)/45$, where P_2 is the second Legendre polynomial of the cosine of the angle θ between the transition dipoles,[59] while that of the $\langle zxxz \rangle$ polarization signal (Figure 3d) is proportional to $P_2/15$. The cross-peak region of the two curves shown in Figure 5 for different polarizations is superimposed on the tail of the diagonal peak. The diagonal peak and the cross-peak in both polarizations were fitted with Gaussian-shaped band profiles to obtain the ratio of $\langle zzzz \rangle_{cross}/\langle zxxz \rangle_{cross}$.

At the acetyl end of NATMA in CH_2Cl_2, the peaks from the different conformers are partially overlapped with one another; thus, the cross peaks between the amino end C═O and the acetyl end C═O of the two conformers could not be resolved in the 2D IR spectrum. The ratio of the areas for the diagonal and the cross peaks was obtained by curve-fitting them separately. The diagonal and cross peaks areas have contributions from both the major and minor conformers. The population of the major conformer is four times the minor one, so it is the ratio $(4\langle zzzz \rangle_1 + \langle zzzz \rangle_2)/(4\langle zxxz \rangle_1 + \langle zxxz \rangle_2)$ (the subscripts 1 and 2 represent the major and minor conformers) that is actually measured. This ratio provides a rough estimate of the angle in the major conformer.

The cross-peak for $\langle zxxz \rangle$ polarization was more intense than that for $\langle zzzz \rangle$ in the 2D IR spectrum of NATMA in methanol at $T = 0$. This ordering is opposite for NATMA in CH_2Cl_2. In the case of NATMA in D_2O, the cross-peak intensities were comparable for both polarization conditions.

The angle between the transition dipoles in CH_2Cl_2 was found to be $112 \pm 5°$ (or $(180-112) \pm 5°$). Similar calculations were made for NATMA in methanol and D_2O, where the angles between the dipoles were found to be $100 \pm 5°$ (or $(180-100) \pm 5°$) and $75 \pm 5°$ (or $(180-75) \pm 5°$).

Coupling between the Amide-I Modes. The off-diagonal anharmonicity was estimated from the relative amplitudes of the diagonal and the cross peaks. Both spectral regions are formed from overlapping positive and negative components whose separation is the anharmonicity. Since the diagonal anharmonicity is readily measurable, the off-diagonal anharmonicity is estimated in a simulation by reducing the separation between two overlapping components until the observed intensity ratio was achieved. An off-diagonal anharmonicity (Δ_{12}) of 2.5 ± 0.5 cm^{-1} was obtained for NATMA in CH_2Cl_2 by this method. This value of Δ_{12} implies a particular coupling between the modes. The assumption in this approach is that the coupling between two modes is the sole source of their mixed mode anharmonicity. On the basis of this assumption, it is a straightforward matrix diagonalization to find the coupling constants (β_{ij}) needed to generate the observed two fundamentals, two overtones, and one combination band based on the known diagonal anharmonicities and the off-diagonal anharmonicity measured by 2D IR.[60] This procedure led to a coupling magnitude of 8 ± 1.0 cm^{-1} for NATMA in CH_2Cl_2. The structure predicted from the calculation of the angles between the two dipoles implies a coupling of 6.5 cm^{-1} based on a dipole−dipole interaction.

For NATMA in methanol and in D_2O, off-diagonal anharmonicities from the foregoing procedure are estimated to be 3.25 ± 0.5 and 3.0 ± 0.5 cm^{-1}, respectively. The corresponding coupling magnitudes are 8.5 ± 1.0 and 5.5 ± 1.0 cm^{-1} respectively. Couplings of 8.0 (methanol) and 5.7 cm^{-1} (D_2O) are obtained from a dipole−dipole interaction assuming structures indicated by the measured angles.

The amide-I coupling magnitudes based on a dipole−dipole interaction and the angles between the transition dipoles were each plotted for a wide range of Ramachandran angles. Comparisons of the experimental results with these plots lead to a number of plausible structures for NATMA in the different solvents. The three-dimensional images of all plausible structures were examined using the molecular and electronic structure viewing program MOLDEN.[61] Some structures were rejected because they had interatomic distances less than the van der Waals separations. In addition the dihedral angles of the dipeptide unit of NATMA were fixed according to the Ramachandran angles of the plausible structures and an energy optimization was performed by means of Gaussian 03[62] by allowing the coordinates of the side chain atoms to vary while keeping the peptide backbone intact. The foregoing rejected structures either did not converge in the Gaussian energy calculation or were of much higher energy content compared with other structures. Structures whose energy calculation did not converge were rejected as were those whose energies exceeded the most stable structures by more than 50 kcal/mol. By combining in this manner the results for the coupling magnitude and the angle between the transition dipoles, the Ramachandran angles for NATMA in CH_2Cl_2 were found to be $(-55 \pm 5°, 30 \pm 5°)$. This result is close to expectations for a C_7 structure with intramolecular hydrogen bonding (Figure 1) between the acetyl end C═O and the *N*-methylamino end N−H. Similar calculations from NATMA in methanol and D_2O

predicts Ramachandran angles of ($120 \pm 10°$, $-20 \pm 10°$) and ($\pm 160 \pm 10°$, $\pm 75 \pm 10°$), respectively. The structure in D_2O is consistent with an open-ended form with no intramolecular hydrogen bonding.

6. Conclusion

Two amide-I bands of NATMA have been assigned unambiguously to the *N*-methylamino and acetyl ends using ^{13}C isotopic substitution. The results lead to the conclusion that the *N*-methylamino end of NATMA has a lower transition frequency in the unlabeled species in CH_2Cl_2 and methanol solutions. However, in D_2O, the acetyl end has a slightly lower transition frequency, evidenced by the fact that with ^{13}C substitution the difference between the acetyl and the amino end transition frequencies is 10 cm^{-1} less in D_2O than in methylene chloride and methanol. The structures of NATMA in all three solvents were estimated from polarization experiments and the anharmonic coupling between the amide-I modes. In CH_2Cl_2, the most stable structure of NATMA was found by 2D IR to be close to a C_7 structure, where the molecule is stabilized by intramolecular hydrogen bonding between the acetyl end C═O and the *N*-methylamino end N−H. This is also one of the most stable structures found by Zwier et al.[51−53] in the gas phase. In D_2O, the major structure was hydrogen-bonded to solvent at both the *N*-methylamino and acetyl ends. The amphiphilic character of NATMA is responsible for its much larger solubility in methanol than in either CH_2Cl_2 or D_2O.

Acknowledgment. This research was supported by the NIH Grant GM12592 and by instrumentation through the Resource RR001348. This paper was originally intended for the C. B. Harris Festschrift [*J. Phys. Chem. B* **2006**, *110*].

References and Notes

(1) Krimm, S.; Bandekar, J. *Adv. Prot. Chem.* **1986**, *38*, 181−364.
(2) Jackson, M.; Mantsch, H. *Crit. Rev. Biochem. Mol. Biol.* **1995**, *30*, 95−120.
(3) Ernst, R. R.; Bodenhausen, G.; Wokaun, A. *Principles of Nuclear Magnetic Resonance in One and Two Dimensions*; Clarendon Press: Oxford, 1987.
(4) Asplund, M. C.; Zanni, M. T.; Hochstrasser, R. M. *Proc. Natl. Acad. Sci. U.S.A.* **2000**, *97*, 8219−8224.
(5) Hamm, P.; Lim, M.; Hochstrasser, R. M. *J. Phys. Chem. B* **1998**, *102*, 6123−6138.
(6) Kim, Y. S.; Hochstrasser, R. M. *Proc. Natl. Acad. Sci. U.S.A.* **2005**, *102*, 11185−11190.
(7) Ding, F.; Fulmer, E. C.; Zanni, M. T. *J. Chem. Phys.* **2005**, *123*, 094502 (1−13).
(8) Zheng, J.; Kwak, K.; Asbury, J.; Chen, X.; Piletic, I. R.; Fayer, M. D. *Science* **2005**, *309*, 1338−1343.
(9) Hamm, P.; Lim, M.; DeGrado, W. F.; Hochstrasser, R. M. *Proc. Natl. Acad. Sci. U.S.A.* **1999**, *96*, 2036−2041.
(10) Woutersen, S.; Hamm, P. *J. Phys. Chem. B* **2000**, *104*, 11316−11320.
(11) Zanni, M. T.; Gnanakaran, S.; Stenger, J.; Hochstrasser, R. M. *J. Phys. Chem. B* **2001**, *105*, 6520−6535.
(12) Hahn, S.; Lee, H.; Cho, M. *J. Chem. Phys.* **2004**, *121*, 1849−1865.
(13) Lee, K.-K.; Hahn, S.; Oh, K.-I.; Choi, J. S.; Joo, C.; Lee, H.; Han, H.; Cho, M. *J. Phys. Chem. B* **2006**, *110*, 18834−18843.
(14) Kim, Y. S.; Wang, J.; Hochstrasser, R. M. *J. Phys. Chem. B* **2005**, *109*, 7511−7521.
(15) Fang, C.; Wang, J.; Charnley, A. K.; Barber-Armstrong, W.; Smith, A. B., III; Decatur, S. M.; Hochstrasser, R. M. *Chem. Phys. Lett.* **2003**, *382*, 586−592.
(16) Fang, C.; Wang, J.; Kim, Y. S.; Charnley, A. K.; Barber-Armstrong, W.; Smith, A. B., III; Decatur, S. M.; Hochstrasser, R. M. *J. Phys. Chem. B* **2004**, *108*, 10415−10427.
(17) Fang, C.; Hochstrasser, R. M. *J. Phys. Chem. B* **2005**, *109*, 18652−18663.
(18) Huang, R.; Kubelka, J.; Barber-Armstrong, W.; Silva, R. A. G. D.; Decatur, S. M.; Keiderling, T. A. *J. Am. Chem. Soc.* **2004**, *126*, 2346−2354.
(19) Ham, S.; Kim, J.-H.; Lee, H.; Cho, M. *J. Chem. Phys.* **2003**, *118*, 3491−3498.
(20) Choi, J.-H.; Ham, S.; Cho, M. *J. Phys. Chem. B* **2003**, *107*, 9132−9138.
(21) Ham, S.; Cho, M. *J. Chem. Phys.* **2003**, *118*, 6915−6922.
(22) Ham, S.; Cha, S.; Choi, J.-H.; Cho, M. *J. Chem. Phys.* **2003**, *119*, 1451−1461.
(23) Choi, J.-H.; Cho, M. *J. Chem. Phys.* **2004**, *120*, 4383−4392.
(24) Choi, J.-H.; Hahn, S.; Cho, M. *Int. J. Quantum Chem.* **2005**, *104*, 616−634.
(25) Kubelka, J.; Huang, R.; Keiderling, T. A. *J. Phys. Chem. B* **2005**, *109*, 8231−8243.
(26) Demirdoven, N.; Cheatum, C. M.; Chung, H. S.; Khalil, M.; Knoester, J.; Tokmakoff, A. *J. Am. Chem. Soc.* **2004**, *126*, 7981−7990.
(27) Cheatum, C. M.; Tokmakoff, A.; Knoester, J. *J. Chem. Phys.* **2004**, *120*, 8201−8215.
(28) Hahn, S.; Kim, S.-S.; Lee, C.; Cho, M. *J. Chem. Phys.* **2005**, *123*, 084905−084910.
(29) Lee, C.; Cho, M. *J. Phys. Chem. B* **2004**, *108*, 20397−20407.
(30) Bour, P.; Keiderling, T. A. *J. Phys. Chem. B* **2005**, *109*, 5348−5357.
(31) Wang, J.; Chen, J.; Hochstrasser, R. M. *J. Phys. Chem. B* **2006**, *110*, 7545−7555.
(32) Bour, P.; Keiderling, T. A. *J. Phys. Chem. B* **2005**, *109*, 23687−23697.
(33) Smith, A. W.; Chung, H. S.; Ganim, Z.; Tokmakoff, A. *J. Phys. Chem. B* **2005**, *109*, 17025−17027.
(34) Hahn, S.; Ham, S.; Cho, M. *J. Phys. Chem. B* **2005**, *109*, 11789−11801.
(35) Maekawa, H.; Toniolo, C.; Moretto, A.; Broxterman, Q. B.; Ge, N.-H. *J. Phys. Chem. B* **2006**, *110*, 5834−5837.
(36) Schweitzer-Stenner, R.; Eker, F.; Huang, Q.; Griebenow, K.; Mroz, P. A.; Kozlowski, P. M. *J. Phys. Chem. B* **2002**, *106*, 4294−4304.
(37) Measey, T.; Hagarman, A.; Eker, F.; Griebenow, K.; Schweitzer-Stenner, R. *J. Phys. Chem. B* **2005**, *109*, 8195−8205.
(38) Eker, F.; Cao, X.; Nafie, L.; Schweitzer-Stenner, R. *J. Am. Chem. Soc.* **2002**, *124*, 14330−14341.
(39) Eker, F.; Griebenow, K.; Cao, X.; Nafie, L. A.; Schweitzer-Stenner, R. *Proc. Natl. Acad. Sci. U.S.A.* **2004**, *101*, 10054−10059.
(40) Thomas Measey, R. S.-S. *J. Raman Spectrosc.* **2006**, *37*, 248−254.
(41) Hayashi, T.; Zhuang, W.; Mukamel, S. *J. Phys. Chem. A* **2005**, *109*, 9747−9759.
(42) Zhuang, W.; Abramavicius, D.; Hayashi, T.; Mukamel, S. *J. Phys. Chem. B* **2006**, *110*, 3362−3374.
(43) Bour, P.; Keiderling, T. A. *J. Chem. Phys.* **2003**, *119*, 11253−11262.
(44) Kubelka, J.; Keiderling, T. A. *J. Phys. Chem. A* **2001**, *105*, 10922−10928.
(45) Cable, J. R.; Tubergen, M. J.; Levy, D. H. *J. Am. Chem. Soc.* **1989**, *111*, 9032−9039.
(46) Cohen, R.; Brauer, B.; Nir, E.; Grace, L.; de Vries, M. S. *J. Phys. Chem. A* **2000**, *104*, 6351−6355.
(47) Snoek, L. C.; Robertson, E. G.; Kroemer, R. T.; Simons, J. P. *Chem. Phys. Lett* **2000**, *321*, 49−56.
(48) Bakker, J. M.; Aleese, L. M.; Meijer, G.; von Helden, G. *Phys. Rev. Lett.* **2003**, *91*, 203003−203004.
(49) Hunig, I.; Seefeld, K. A.; Kleinermanns, K. *Chem. Phys. Lett* **2003**, *369*, 173−179.
(50) Unterberg, C.; Gerlach, A.; Schrader, T.; Gerhards, M. *J. Chem. Phys.* **2003**, *118*, 8296−8300.
(51) Dian, B. C.; Longarte, A.; Winter, P. R.; Zwier, T. S. *J. Chem. Phys.* **2004**, *120*, 133−147.
(52) Dian, B. C.; Longarte, A.; Mercier, S.; Evans, D. A.; Wales, D. J.; Zwier, T. S. *J. Chem. Phys.* **2002**, *117*, 10688−10702.
(53) Evans, D. A.; Wales, D. J.; Dian, B. C.; Zwier, T. S. *J. Chem. Phys.* **2004**, *120*, 148−157.
(54) Souhassou, M.; Lecomte, C.; Blessing, R. H.; Aubry, A.; Rohmer, M.-M.; Wiest, R.; Benard, M.; Marraud, M. *Acta Crystallogr., Sect. B: Struct. Sci.* **1991**, *47*, 253−266.
(55) Zanni, M. T.; Gnanakaran, S.; Stenger, J.; Hochstrasser, R. M. *J. Phys. Chem. B* **2001**, *105*, 6520−6535.
(56) Kwac, K.; Cho, M. *J. Phys. Chem. A* **2003**, *107*, 5903−5912.
(57) Kwac, K.; Cho, M. *J. Chem. Phys.* **2003**, *119*, 2256−2263.
(58) Ge, N.-H.; Zanni, M. T.; Hochstrasser, R. M. *J. Phys. Chem. A* **2002**, *106*, 962−972.
(59) Hochstrasser, R. M. *Chem. Phys.* **2001**, *266*, 273−284.
(60) Hamm, P.; Hochstrasser, R. M. In *Ultrafast Infrared and Raman Spectroscopy*; Fayer, M. D., Ed.; Marcel Dekker, Inc.: New York, 2001; p 273.
(61) Schaftenaar, G.; Noordik, J. H. *J. Comput.-Aided Mol. Design* **2000**, *14*, 123−134.

(62) Frisch, M. J.; Trucks, G. W.; Schlegel, H. B.; Scuseria, G. E.; Robb, M. A.; Cheeseman, J. R.; Montgomery, J. A., Jr.; Vreven, T.; Kudin, K. N.; Burant, J. C.; Millam, J. M.; Iyengar, S. S.; Tomasi, J.; Barone, V.; Mennucci, B.; Cossi, M.; Scalmani, G.; Rega, N.; Petersson, G. A.; Nakatsuji, H.; Hada, M.; Ehara, M.; Toyota, K.; Fukuda, R.; Hasegawa, J.; Ishida, M.; Nakajima, T.; Honda, Y.; Kitao, O.; Nakai, H.; Klene, M.; Li, X.; Knox, J. E.; Hratchian, H. P.; Cross, J. B.; Bakken, V.; Adamo, C.; Jaramillo, J.; Gomperts, R.; Stratmann, R. E.; Yazyev, O.; Austin, A. J.; Cammi, R.; Pomelli, C.; Ochterski, J. W.; Ayala, P. Y.; Morokuma, K.; Voth, G. A.; Salvador, P.; Dannenberg, J. J.; Zakrzewski, V. G.; Dapprich, S.; Daniels, A. D.; Strain, M. C.; Farkas, O.; Malick, D. K.; Rabuck, A. D.; Raghavachari, K.; Foresman, J. B.; Ortiz, J. V.; Cui, Q.; Baboul, A. G.; Clifford, S.; Cioslowski, J.; Stefanov, B. B.; Liu, G.; Liashenko, A.; Piskorz, P.; Komaromi, I.; Martin, R. L.; Fox, D. J.; Keith, T.; Al-Laham, M. A.; Peng, C. Y.; Nanayakkara, A.; Challacombe, M.; Gill, P. M. W.; Johnson, B.; Chen, W.; Wong, M. W.; Gonzalez, C.; Pople, J. A. *Gaussian 03*, Revision C.02; Gaussian, Inc.: Wallingford, CT, 2004.